Deliverable D11.1
WP11 — JRA05

Benchmarking of the event generator for light-ion induced reactions

Sylvie Leray,[1] **Davide Mancusi**,[1] Alain Boudard,[1] Joseph Cugnon,[2] Jean-Christophe David,[1] and Pekka Kaitaniemi[1]

[1] *CEA, Centre de Saclay, Irfu/SPhN, F-91191 Gif-sur-Yvette, France*
[2] *Fundamental Interactions in Physics and Astrophysics, University of Liège, allée du 6 août 17, bât. B5, B-4000 Liège 1, Belgium*

I. INTRODUCTION

The Liège intranuclear-cascade model (INCL) [1, 2], jointly developed by CEA-Saclay (France) and the University of Liège (Belgium), has been established as an accurate tool for the description of nucleon- and pion-induced reactions on nuclei between ∼100 MeV and ∼3 GeV [3]. When coupled to a suitable nuclear de-excitation model, it can reliably reproduce several observables such as emission spectra of particles and light ions, residual mass and charge distributions and residual recoil-velocity distributions. Since the precursor INCL code is written in Fortran, it is unsuitable for inclusion in Geant4 [4, 5], a flexible C++ toolkit for the simulation of particle transport in matter.

This report presents INCL++, a completely redesigned version of the INCL model in C++, now available in Geant4. The new C++ version of INCL is the starting point for an extension to reactions induced by light nuclei. We shall present the general ideas and difficulties connected with the extension and demonstrate the quality of the model predictions by comparing against selected experimental data and other Geant4 reaction models.

Throughout this document, we will refer to the INCL++ version 5.1.14, which is distributed along with the latest stable Geant4 version (10.0).

II. EXTENSION TO LIGHT-ION-INDUCED REACTIONS

It has been demonstrated [3] that the Liège Intranuclear Cascade model can successfully reproduce a vast set of observables pertaining to nucleon-induced ($N + A$) reactions between a few tens of MeV and a few GeV, which suggests that the model condenses the physics that is essentially relevant in this energy range. It is therefore natural to take it as a starting point for the development of a new model for light-ion-induced reactions ($A + A$).

We briefly mention here that an INCL-based extension to $A + A$ reactions has already been attempted [6] on the basis of an old version of the model (INCL4.3). We shall not dwell on the differences between the two approaches here, mostly because the model described in the present work is more sophisticated in several respects and should be considered as the reference point for any future development.

The treatment of $A + A$ reactions in an INC framework poses several challenges which do not apply to $N + A$ reactions. Most importantly, there is no natural way of accounting for the binding of the projectile nucleus within the INC scheme. The cascade takes place in a single mean-field potential, which is typically assumed to be that of the target nucleus; this essentially amounts to neglecting the mean-field interaction between the projectile constituents. It is clear that no model can describe projectile fragmentation if the binding of the projectile nucleons is neglected.

A. Projectile binding and Lorentz boost

We try to deal with this limitation using a semi-empirical projectile-preparation algorithm, which we now turn to describe. We shall limit ourselves to an outline of the most important assumptions, leaving a detailed description to a future publication.

We choose to account for the projectile binding by putting the A_p projectile nucleons off their mass shell. Let π_i be the momentum of the i-th projectile nucleon in the projectile center of mass (drawn from some appropriate

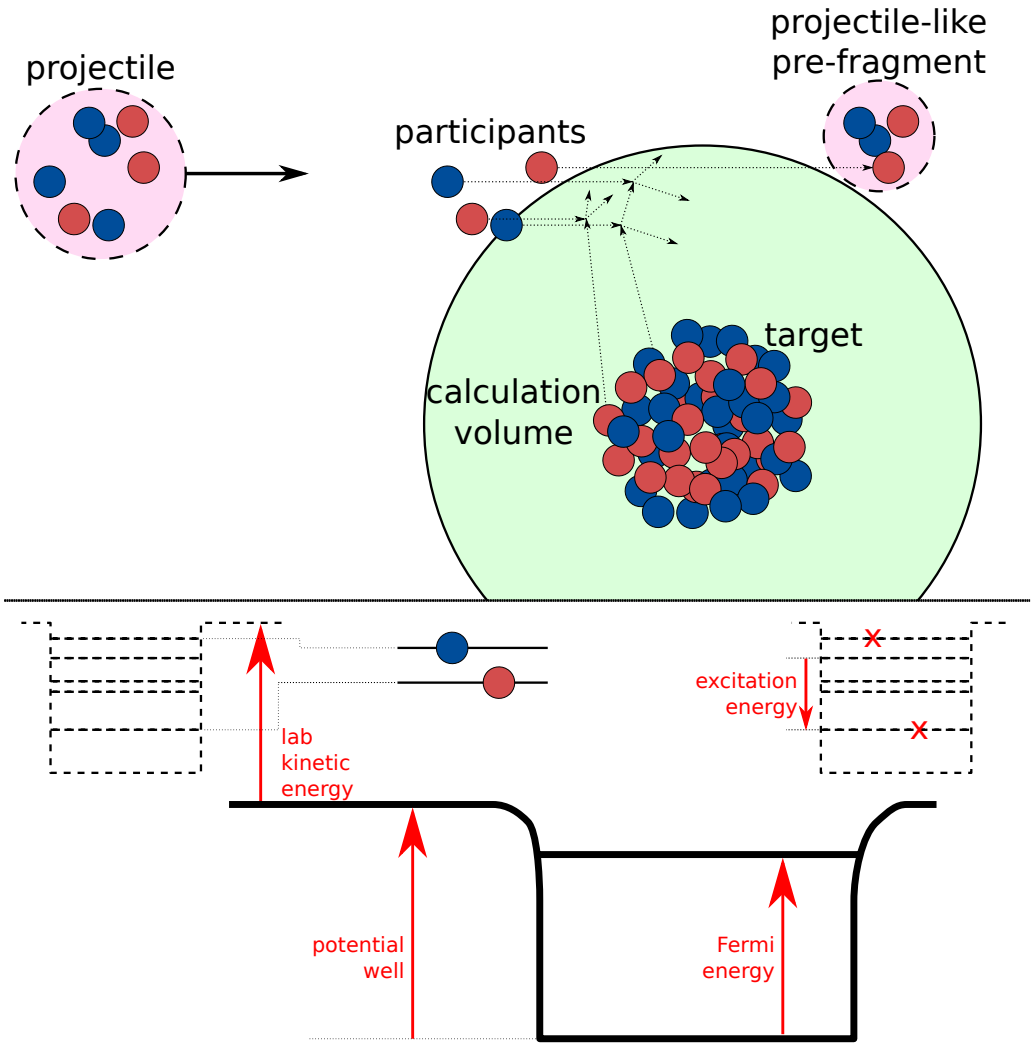

Figure 1: Schematic depiction of the preparatory phase of a nucleus-nucleus reaction in INCL++.

distribution), M_p the mass of the projectile nucleus and m = 938.2796 MeV the mass of the INCL nucleon; we define the *dynamical pseudopotential* of the projectile as

$$V_p = A_p^{-1}\left[\sum_i \sqrt{\pi_i^2 + m^2} - M_p\right].$$

This quantity has the dimensions of an energy, is always positive, and can be interpreted as the opposite of the average potential energy that the nucleons must feel if their total relativistic energy is to be equal to the nominal mass of the projectile. Note that V_p is a random variable because it depends on the values of the drawn nucleon momenta.

We define the nucleon relativistic energies in the center of mass as

$$\varepsilon_i = \sqrt{\pi_i^2 + m^2} - V_p. \tag{1}$$

The four-momenta of the projectile nucleons $(\varepsilon_i, \boldsymbol{\pi}_i)$ are not on mass shell; however, they satisfy energy- and momentum-balance relations that are appropriate for the center of mass of the projectile, namely:

$$\sum \varepsilon_i = M_p, \tag{2a}$$

$$\sum \boldsymbol{\pi}_i = 0. \tag{2b}$$

The four-momenta of the projectile nucleons in the laboratory frame $(e_i, \boldsymbol{p}_i)$ are defined by a Lorentz boost on the CM four-momenta, parametrised by the nominal Lorentz parameters of the beam. Eqs. (2) guarantee that the energy

and momentum balance are correct:

$$\sum e_i = E_p \tag{3a}$$

$$\sum \boldsymbol{p}_i = \boldsymbol{P}_p. \tag{3b}$$

The positions of the nucleons in the laboratory frame are defined to take into account Lorentz contraction along the z axis.

Summarizing, the procedure outlined above defines positions and four momenta for the A_p projectile nucleons in the laboratory frame. The sum of the nucleon four-momenta is equal to the nominal four-momentum of the projectile nucleus. However, the nucleon four-momenta are off mass shell.

The initial positions of the nucleons with respect to the target nucleus are defined by the impact parameter and by an algorithm which takes into account the Coulomb deviation of the projectile trajectory. The procedure used in INCL++ closely resembles the one used in INCL4.6 [1], to which the reader is referred. The result of the algorithm is to define entrance positions and times for all projectile nucleons into the calculation sphere.

B. Intranuclear-cascade phase

An important ingredient of the nucleus-nucleus extension is the assumption that projectile nucleons propagate with the (Coulomb-distorted) collective velocity of the projectile beam until they undergo a collision. This has two consequences. First, projectile nucleons can immediately be divided in two classes: those whose trajectory intersects the INCL "working sphere" are labelled as *geometrical participants*; the others are called *geometrical spectators*. If there are no geometrical participants, the event is considered as transparent (no reaction). Second, the entrance times of the geometrical participants in the calculation volume can be analytically predicted. The entrance time of the first nucleon is taken as the starting time of the intranuclear cascade. Figure 1 schematically depicts the preparatory phase.

The intranuclear-cascade phase starts with one of the projectile nucleons entering the calculation volume. This event can actually be seen as the transfer of a nucleon from the projectile to the target nucleus. If we seek to conserve energy during the whole intranuclear-cascade phase, the Q-value for nucleon transfer must somehow be taken into account in the treatment of the incoming nucleon. In the context of nucleon-induced reactions, this observation has led us to introduce experimental thresholds for particle emission [1]: the energies of particles entering and leaving the nucleus are adjusted to match the experimental Q-values for particle emission and absorption. In nucleus-nucleus reactions, the situation is complicated by the possibility that nucleon transfer from the projectile to the target leaves the projectile in an excited state. However, the intranuclear-cascade model does not offer any natural prescription to fix the excitation energy of the projectile-like pre-fragment. Therefore, we need to resort to an additional model. In what follows, we assume that removal of nucleons from the projectile leads to a particle-hole-like excitation energy. More precisely, assume that only the A nucleons labeled by $i = 1, \ldots, A$ are left in the projectile; then the excitation energy can be defined as

$$E^*_A = \sum_{j=1}^{A} \varepsilon_j - \sum_{j=1}^{A} \varepsilon_{i_j}. \tag{4}$$

Here the second summation is intended to run over the A smallest values of the CM energies ε_i (Eq. (1)), which are collectively meant to represent a reference state for the A-nucleon pre-fragment. The excitation energy is computed as the difference between the total energy left in the pre-fragment CM and the energy of the reference state. It has the desirable property of always being non-negative.

When the first projectile nucleon enters the calculation volume, its kinetic energy is adjusted to satisfy the global energy-conservation balance, which involves the target mean-field potential, the excitation energy of the projectile and the transfer Q-value. As customary, it is assumed that cascading nucleons are on mass shell. Therefore, once the energy is determined, the magnitude of the nucleon momentum inside the target potential is defined by the on-shell dispersion relation.

We draw the attention of the reader to an important detail. As long as the nucleon has not undergone any collision, it is taken to propagate inside the target potential with the *collective* velocity of the projectile nucleus, regardless of the direction of its momentum. The nucleon four-momentum is however correctly used in the computation of the elementary cross sections and in the kinematics of the binary collisions. Once the nucleon has experienced a (non-Pauli-blocked) binary collision, normal propagation is resumed.

The intranuclear cascade unfolds normally until another projectile nucleon reaches the surface of the calculation volume. The procedure outlined above is then applied to the new nucleon and normal cascade is resumed. Once all the nucleons have entered the calculation volume, the usual conditions for cascade stopping apply [1].

At the end of the intranuclear cascade, a projectile pre-fragment may be defined if some nucleons missed the calculation volume (geometrical spectators) or traversed the calculation volume without undergoing any collision (dynamical spectators). If no dynamical spectators are present, the mass, charge, excitation energy and state of motion of the projectile pre-fragment are already defined (see e.g. Eq. (4) above). If there are dynamical spectators, we tentatively define the pre-fragment four-momentum as the sum of the four-momenta of the dynamical and geometrical spectators. If the resulting four-momentum leads to a negative excitation energy, the code determines the maximal number of dynamical spectators that can be incorporated in the pre-fragment without leading to negative excitation energy. The end result of this procedure is always a projectile-like pre-fragment with non-negative excitation energy.

C. Projectile-target asymmetry

One of the weaknesses of the light-ion extension here described is that it clearly introduces a projectile-target asymmetry. While the projectile nucleus is essentially treated as a collection of free off-mass-shell nucleons, the target nucleus is endowed with a mean-field potential that is able to actually bind nucleons that participated in the reaction. The reader should also contrast the excitation energy assigned to the projectile-like pre-fragment, which is based on a simple particle-hole model, with that assigned to the target-like pre-fragment, which results from and carries information about the full INC dynamics.

One practical consequence is that the cross sections for producing a given nuclide as a projectile-like fragment or as a target-like fragment will in general not be equal. One would reasonably expect that the predictions for target-like fragment production should be closer to the experimental data, given the superior physical modeling of the target nucleus. If projectile-like fragmentation is more important than target-like fragmentation for a specific application, and if both reaction partners are light ions, one can consider swapping the roles of projectile and target in the simulation: in other words, the reaction can be simulated in inverse kinematics (i.e. as target on projectile), with the reaction products being boosted back to the laboratory frame at the end of the simulation. We refer to this calculation method as *accurate-projectile mode*, while we use the expression *accurate-target mode* to refer to the normal INCL++ calculation mode. We shall illustrate the differences between the two calculation modes in the following section.

We should stress that the choice between accurate-target and accurate-projectile mode is application-dependent. If the user is interested e.g. in projectile-like fragments for radiation-protection and hadrontherapy simulations, they should use accurate-projectile mode. A universal choice is not possible; however, we believe that accurate-projectile mode provides a better description of particle transport for several applications where INCL++ is likely to give accurate results. Therefore, Geant4 uses INCL++ in projectile-accurate mode by default. The user can switch to target-accurate mode using the `/process/had/inclxx/accurateNucleus` macro.

D. Low-energy fusion model

So far we have implicitly assumed that the transfer of one nucleon from the projectile to the target is always possible. However, serious conceptual and technical complications arise if the kinetic energy of one of the entering nucleons is lower than the Fermi energy of the target. This difficulty has already been encountered in the extension of INCL4.6 to light incident clusters [1]. For problematic events, INCL4.6 abandons normal INC in favor of a simple geometrical fusion model. The details of the fusion model implemented by INCL++ are slightly different because it needs to be applied to a wider range of projectiles (up to $A = 18$). We reserve a thorough discussion of the differences to a future publication.

III. VALIDATION OF THE NUCLEUS-NUCLEUS EXTENSION

A. Reaction cross sections

We now turn to the validation of the capability to handle $A + A$ reactions. Figure 2 shows an excitation function for the $^{12}C+^{12}C$ reaction cross section. The agreement with the experimental data is not very good. More precisely, we can observe that the double-humped INCL++ excitation function clearly exhibits two distinct regimes. The low-energy peak (around 5 *A*MeV) is due to the fusion model. In fact, pure INC plays essentially no role as long as at least one projectile nucleon enters the calculation sphere below the Fermi energy. The importance of the fusion mechanism starts to decrease above 5 *A*MeV and gradually leaves the place to the pure INC mechanism, which is responsible for the second peak (around 70 *A*MeV).

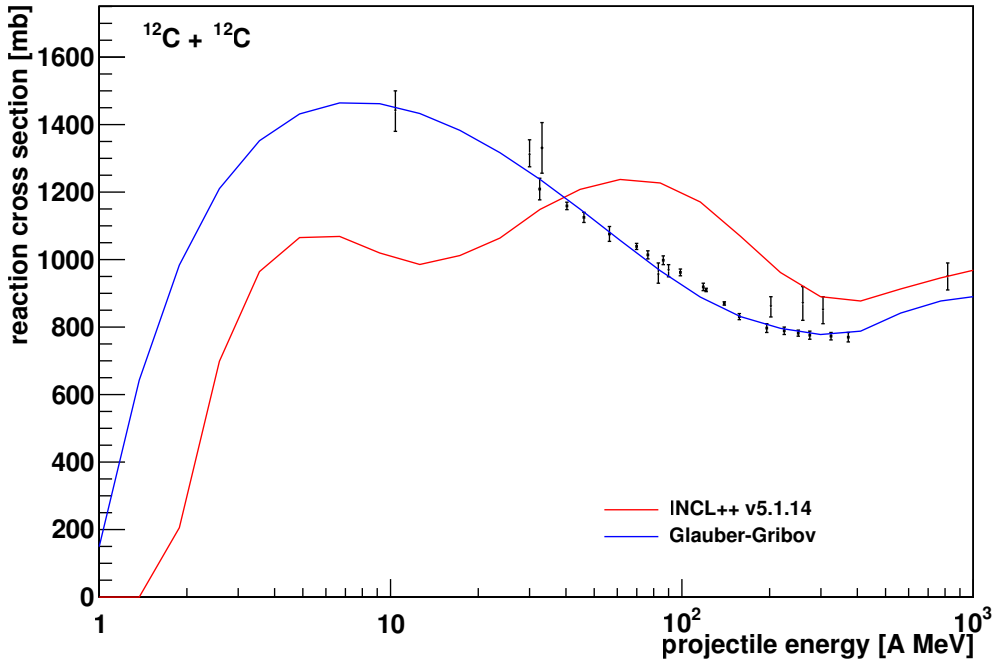

Figure 2: Excitation function for the ^{12}C+^{12}C reaction cross section, calculated with INCL++ (red line) and Geant4's Glauber-Gribov semi-empirical reaction-cross-section model (blue line). Experimental data taken from Refs. 7–12.

Particle transport in Geant4 is not seriously affected by this deficiency, because the reaction cross section is imposed during the transport step; however, the disagreement clearly indicates a failure to correctly describe the physics of this reaction, especially at low energy. It might be argued that the ^{12}C+^{12}C reaction does not represent a fair benchmark for intranuclear-cascade models, which assume that the larger reaction partner is left relatively unperturbed by the cascade; however, it is necessary to make sure that the model yields reasonable results in this domain in view of the large importance of this and other similar reactions for medical applications.

Note that the INC approximation is expected to be valid above some 150 *A*MeV. In this energy range, the contribution from the (admittedly empirical) fusion sector is negligible, thereby simplifying the interpretation of the resulting cross section. We see that the model overestimates the experimental data by about 15%; we believe this is due to the fact that we neglect Pauli blocking of the first collision in the Fermi sea of the projectile. This analysis is corroborated by the observation that the nucleon-^{12}C reaction cross sections are correctly predicted in the same range of energy per nucleon [1]. The extent of the expected suppression is also roughly compatible with the known effect of Pauli blocking on nucleon-nucleus reactions.

B. Caveat about cross-section normalization

Before turning to double-differential cross sections for particle production, a word of caution should be said about the comparisons shown in the following sections between INCL++ and the other models available in Geant4. Most nuclear-reaction models are able to predict absolute reaction cross sections; however, these quantities are not directly used in particle transport, because more accurate semi-empirical parametrizations are usually available. Nevertheless, a misprediction of the reaction cross section might indicate that the model fails to describe some particular channel. We try to make our point clearer by referring to Fig. 2 above. We claimed that the overprediction of the ^{12}C+^{12}C reaction cross section at high energy is due to the lack of Pauli blocking on the first collision in the projectile Fermi sea. If our conjecture is correct, this defect should mostly lead to an overestimation of the cross sections associated with peripheral collisions. Therefore, even though the gross overestimation is only 15% of the reaction cross section, the relative overprediction might be much more conspicuous in channels associated with peripheral collisions.

The Geant4 nuclear-reaction models discussed below (QMD, BIC, Bertini+PreCompound) are only accessible through their Geant4 interface classes. Because of the way nuclear-reaction models are used in particle transport, the interfaces iterate calls to the model engine until an inelastic event is generated. Therefore, the absolute reaction cross sections predicted by the Geant4 models are *not* available to us. We chose to normalize the raw model predictions (counts) using the Shen nucleus-nucleus cross section [13], which is available in Geant4 through class

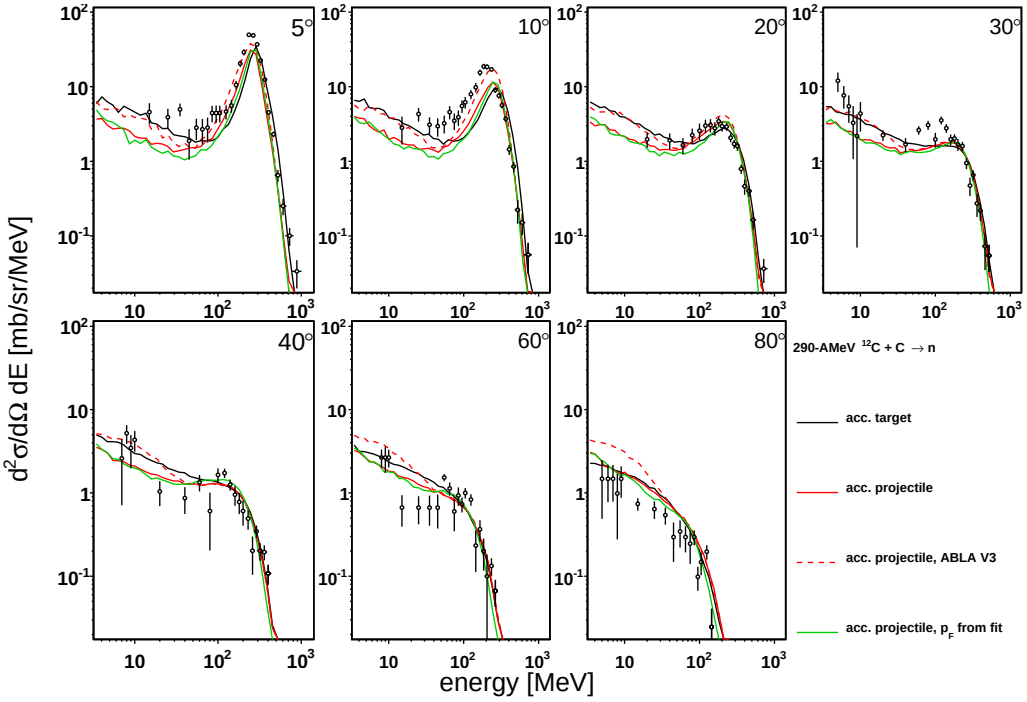

Figure 3: Double-differential cross sections for neutron production from a 290-*A*MeV ^{12}C+C reaction. The INCL++ calculations are presented in accurate-target (black lines) and accurate-projectile (red solid lines) mode, coupled with the G4ExcitationHandler de-excitation model. We also show an accurate-projectile calculation with ABLA V3 (red dashed lines) and a calculation with a modified value of the Fermi momentum (green lines, see text). Experimental data are taken from Ref. 14.

G4IonsShenCrossSection.

Note that this inevitable complication is of little concern for particle-production cross sections (Sec. III C), which often span several orders of magnitude. Fragmentation cross sections (Sec. III D) are more sensitive. For simplicity, we have chosen to keep INCL++'s intrinsic normalization everywhere, *except* for fragmentation cross sections (Figs. 12–19), where we normalized the INCL++ predictions using the ratio of Shen's reaction cross section to INCL++'s intrinsic reaction cross section. The ratio was in all cases between 0.8 and 1.

C. Particle-production cross sections

Figure 3 demonstrates the difference between accurate-projectile and accurate-target mode (see Section II C) using double-differential cross sections for neutron production from the 290-*A*MeV ^{12}C+C [14] and 230-*A*MeV ^{4}He+Cu [15] reactions. Note that the incident energy is large enough in both cases so that the low-energy fusion sector can be neglected. Both calculations were coupled to the native Geant4 de-excitation model [16]. Differences are mostly visible at forward angles; the predictions for the largest angles are very close to each other, especially for the ^{4}He-induced reaction. In general, the shapes of the experimental spectra are quite well reproduced by both INCL++ calculations. Therefore, we conclude that nucleon emission is nevertheless projectile-target symmetric to a good degree.

Note that the experimental data show a peak at forward angles roughly centered around the nominal energy per nucleon of the projectile and correspond to neutrons with a rather small energy in the projectile rest frame. In INCL++, they mainly originate from the break-up of the projectile nucleus. The shape and the height of the peak depend on the selected de-excitation model; this is illustrated again by Fig. 3, where the accurate-projectile calculation coupled with G4ExcitationHandler(which for this system reduces to Fermi break-up) is contrasted to an INCL++/ABLA V3 calculation (solid and dashed red lines, respectively). The ABLA V3 model yields a larger, broader peak, in better agreement with the experimental data at forward angles, but also affects the low-energy neutron yields at large angles.

The shape of the projectile-fragmentation peak is also sensitive to the assumed Fermi momentum of the projectile nucleus. This is illustrated by an accurate-projectile INCL++ calculation using a mass-dependent Fermi momentum

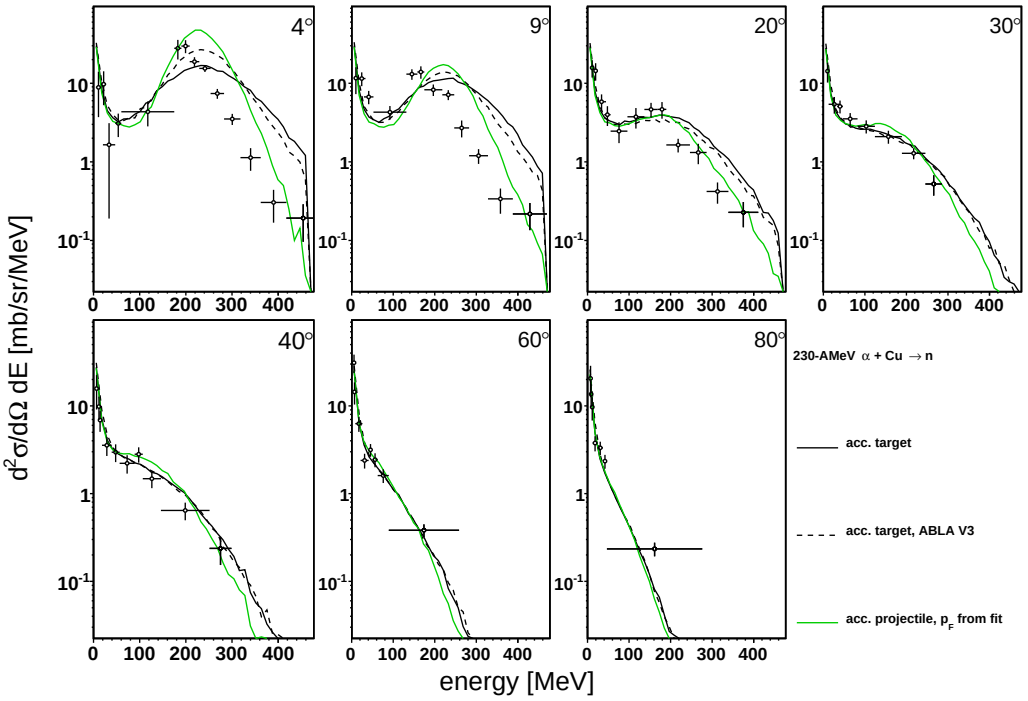

Figure 4: Same as Fig. 3, for the 230-*A*MeV ^{4}He+Cu reaction. Experimental data are taken from Ref. 15.

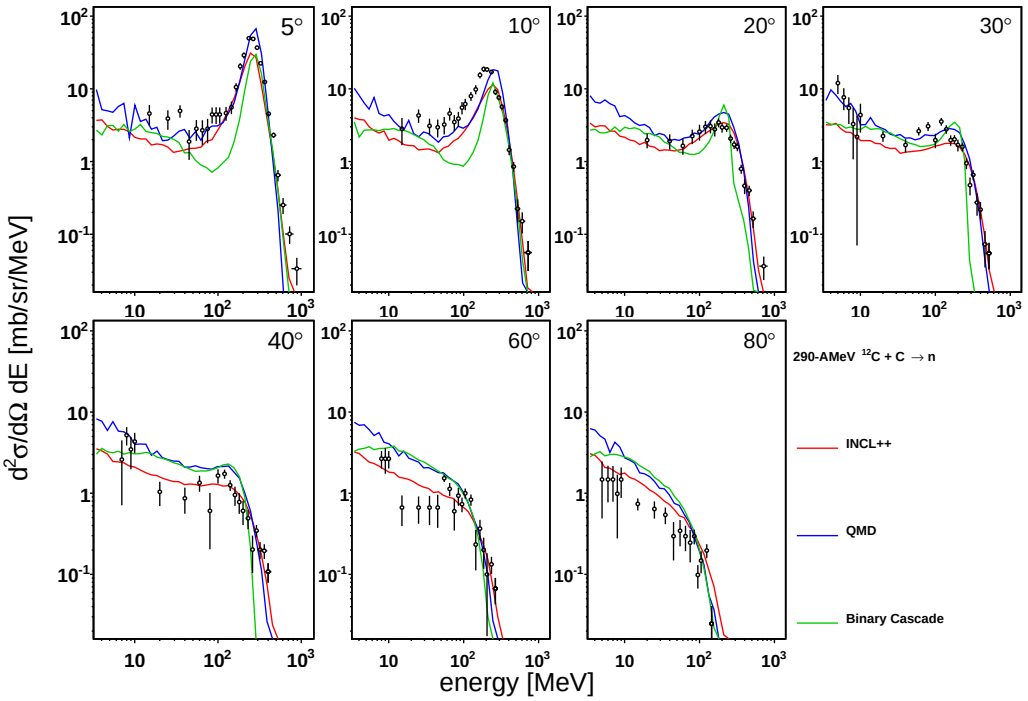

Figure 5: Same as Fig. 3 for INCL++ (accurate-projectile mode, red lines), Geant4's QMD model (blue lines) and BIC model (green lines).

given by

$$p_F(A) = \alpha - \beta \exp(-\gamma A)$$
$$\alpha = 259.416\ \text{MeV}/c, \quad \beta = 152.824\ \text{MeV}/c, \quad \gamma = 9.5157 \cdot 10^{-2}.$$

This formula is a fit to Moniz et al.'s direct measurements by quasi-elastic electron scattering [17]. For ^{12}C, the formula yields $p_F(^{12}\text{C}) \simeq 210\ \text{MeV}/c$ (Moniz et al.'s measurement is actually $(221 \pm 5)\ \text{MeV}/c$), which is not very

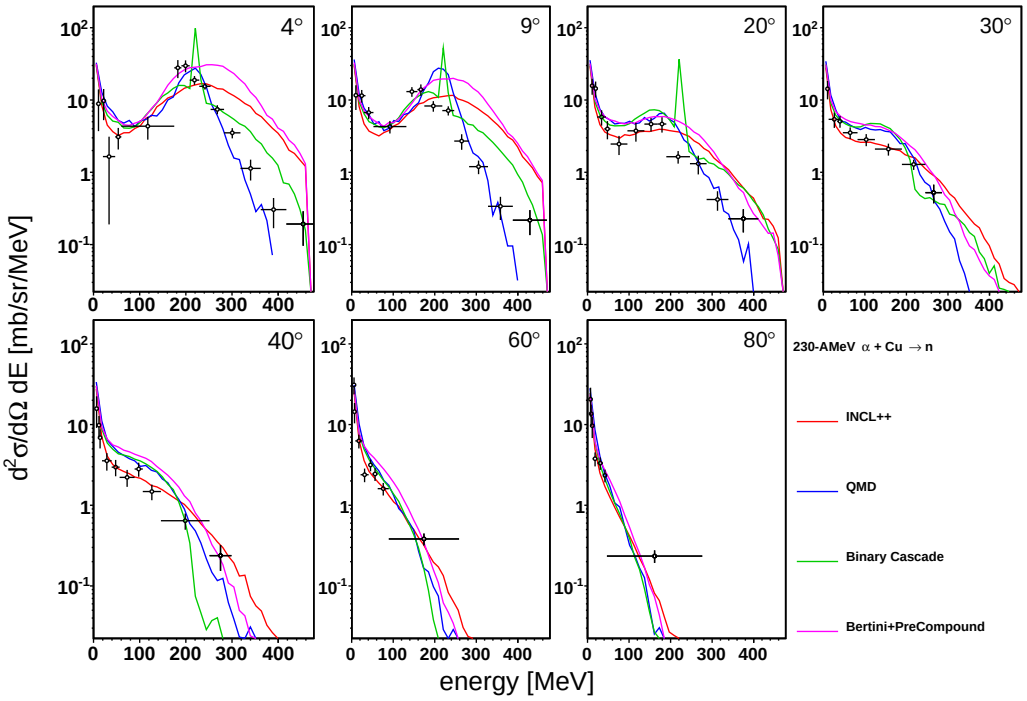

Figure 6: Double-differential cross sections for neutron production from the 230-*A*MeV ^{4}He+Cu reaction. Same color code as Figure 5; predictions of Bertini+PreCompound are represented by purple lines. Experimental data are taken from Ref. 15.

different from the default INCL++ value of 270 MeV/c. Nevertheless, Fig. 3 shows that the neutron spectra are roughly equally sensitive to the de-excitation model and to the Fermi momentum.

The sensitivity to p_F can be enhanced by looking at lighter projectiles, such as ^{4}He in the 230-*A*MeV ^{4}He+Cu reaction depicted in Fig. 4. Here $p_F(^4\text{He}) = 155\ \text{MeV}/c$, almost a factor of two smaller than the nominal INCL++ value. For this system, standard INCL++ fails to describe the part of the spectrum above 200 MeV. However, the projectile-fragmentation peak at forward angles is much better reproduced using the empirical Fermi momentum. Nevertheless, since we have not extensively tested the implications of empirical Fermi momenta in INCL++, we keep $p_F = 270\ \text{MeV}/c$ as the default value. We reserve a detailed study to a future publication.

Figures 3 and 4 suggest that INCL++ generally succeeds to capture the essential aspects of the experimental data. This conclusion is corroborated by Figures 5 and 6, which show a comparison of the INCL++ result (in accurate-projectile mode) to calculations performed by other models available in Geant4: QMD model (blue), BIC [18] (green) and Bertini+PreCompound [19–21] (purple, only applicable for the ^{4}He-induced reaction). All models use the same de-excitation (G4ExcitationHandler), except Bertini, which has its own internal de-excitation module.

One notices that the BIC predictions are generally in less good agreement with the experimental data than INCL++. The QMD results are everywhere comparable to or worse than the INCL++ calculation, except at the forward-most angles, which were shown to be improvable in INCL++ by using the empirical Fermi momentum. Note also that the CPU time for QMD is one to two orders of magnitude larger than for INCL++. All the other models fail to describe the ^{4}He-fragmentation peak, which (in view of the above) might suggest that they employ unrealistic Fermi momenta for the this projectile. In addition, the BIC model shows some unphysical structures at small angles for the ^{4}He+Cu system.

We now turn to the production of charged particles. We focus in particular on a recent experiment by Dudouet *et al.* [22, 23], who measured double-differential cross sections for the production of several charged particles from reactions induced by a 95-*A*MeV ^{12}C beam on targets ranging from hydrogen to titanium. We are mostly interested in the carbon-target data for the purpose of validating the INCL++ nucleus-nucleus extension and assessing the severity of the projectile-target asymmetry. Calculations with some Geant4 models have been presented in Ref. 24, where however the authors of used an old version of INCL++ that was shown above to be affected by serious bugs for the ^{12}C+^{12}C reaction (Fig. 2). Our results can be reproduced using Geant4 v10.0 and should be considered as references.

First, we observe that the incident energy (95 *A*MeV) is rather low. The conditions for the applicability of the intranuclear-cascade hypothesis (independent binary nucleon-nucleon collisions) are not very well fulfilled here. Figure 2 indicates that the reaction cross section predicted by INCL++ is in excess of the experimental value by about 30% at this energy. Note also that INCL++'s low-energy fusion sector is responsible for 43% of the reaction

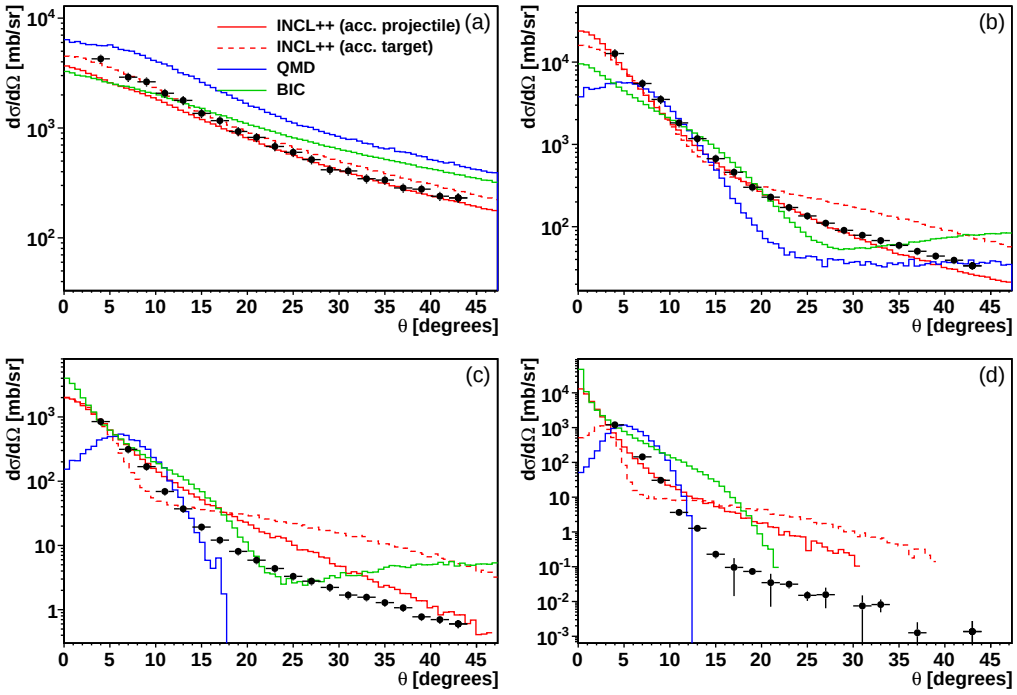

Figure 7: Angle-differential cross section for the production of (a) protons, (b) ^{4}He, (c) ^{7}Li and (d) ^{11}C from the 95-*A*MeV ^{12}C+^{12}C reaction. Calculations with INCL++ (accurate-projectile mode, solid red lines; accurate-target mode, dashed red lines), QMD (blue lines) and BIC (green lines) are shown. Experimental data are taken from Ref. 22.

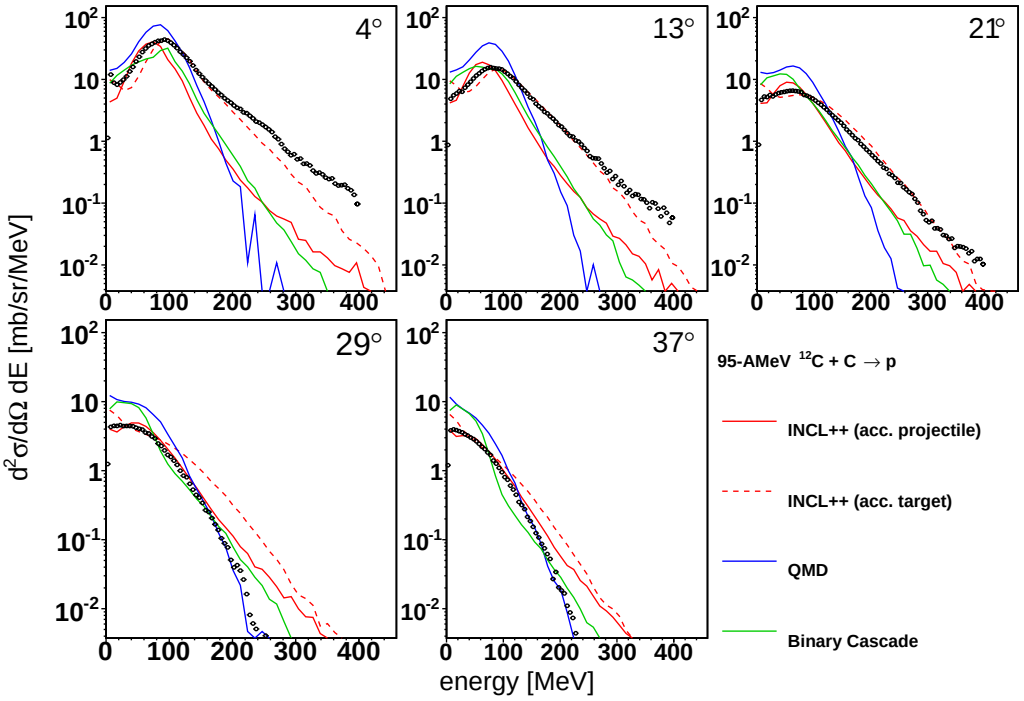

Figure 8: Double-differential cross sections for the production of protons from the 95-*A*MeV ^{12}C+^{12}C reaction. Calculations with INCL++ (accurate-projectile mode, solid red lines; accurate-target mode, dashed red lines), QMD (blue lines) and BIC (green lines) are shown. Experimental data are taken from Ref. 22.

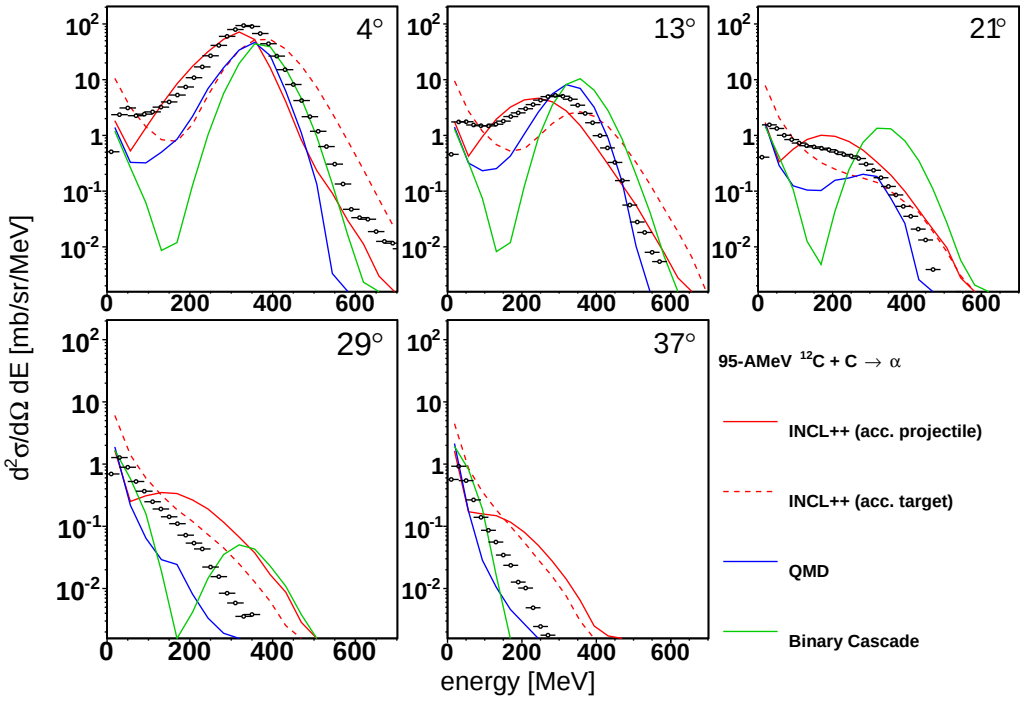

Figure 9: Same as Fig. 8, for ^{4}He ejectiles.

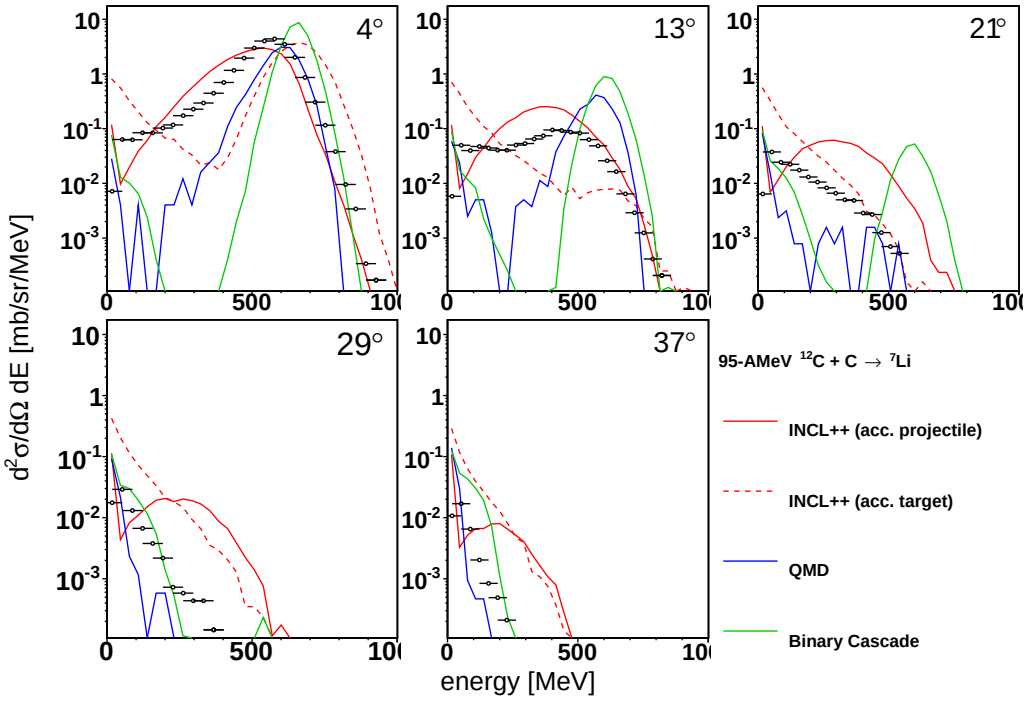

Figure 10: Same as Fig. 8, for ^{7}Li ejectiles.

cross section, which is far from negligible. Given the empirical nature of the fusion sector, we do not expect very accurate predictions.

Figure 7 shows angular-differential cross sections for the production of protons, ^{4}He, ^{7}Li and ^{11}C. For each angle, the calculated ejectile energy distributions were integrated above the detection thresholds reported by Dudouet *et al.* [Table IV in 23].

It is striking that none of the considered models can accurately reproduce all the experimental data. The proton angular distributions predicted by INCL++ (either in accurate-projectile or in accurate-target mode) are quite close to the experimental data; the accurate-projectile and accurate-target predictions are again very similar, which confirms

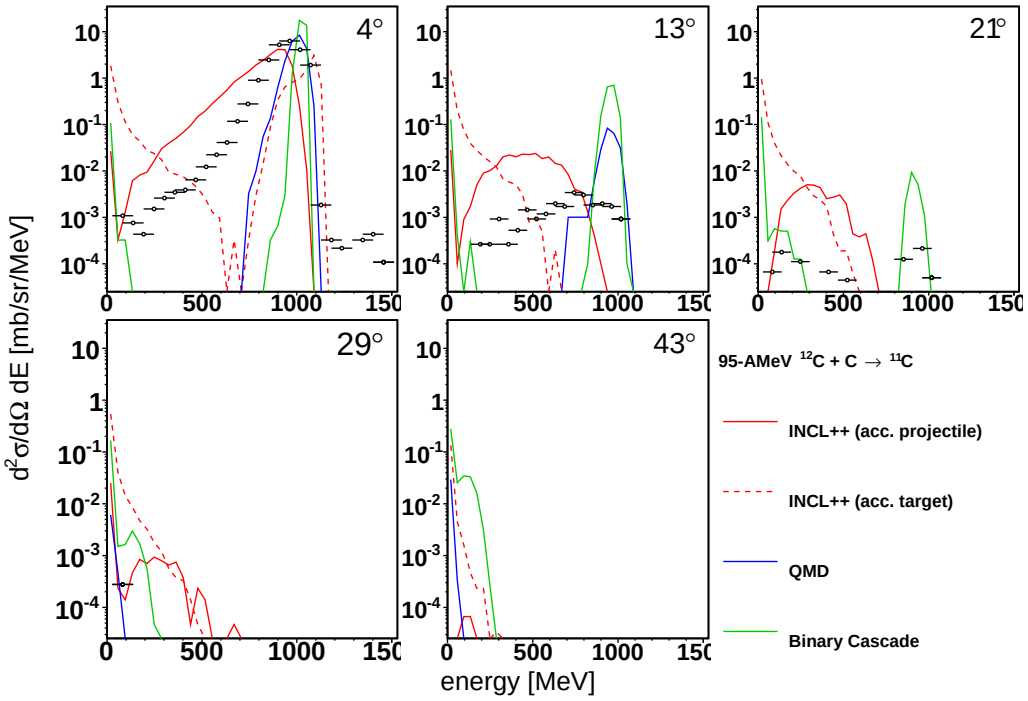

Figure 11: Same as Fig. 8, for ^{11}C ejectiles.

the remark made about Fig. 3.

The agreement progressively degrades as the mass of the ejectile increases, especially for the calculation in accurate-target mode. Dudouet *et al.* [23] showed that the experimental angular distributions can be represented as a sum of a Gaussian and an exponential contribution and claimed [24] that no model can reproduce this trend. Figure 7 shows that this is incorrect: although the exponential tail of the angular distribution might be quantitatively incorrect (especially for ^{11}C), INCL++ in accurate-projectile mode is clearly the only model that can capture the trend of the experimental data. In spite of the crudeness of the model ingredients, the agreement with the experimental data is remarkable, except for the case of ^{11}C. As we mentioned above (Sec. III B), this might be connected with the lack of Pauli blocking on the first collision in the projectile, which probably leads to an overestimation of the probability for the removal of few nucleons from the projectile and the target.

As far as the other models are concerned, QMD seems to systematically underpredict the fragment yields at small angles. In general, the shape of the angular distribution is very different from the experimental result. Even for protons one can observe a sizable overestimation of the yield. The BIC results manage to capture at least some qualitative features of the experimental data, but its overall predictions are in worse agreement than INCL++'s.

Double-differential spectra for the same ejectiles are shown in Figs. 8–11. Here we notice larger discrepancies than in Fig. 7, even for the INCL++ calculation in accurate-projectile mode. For example, no model can reproduce the slope of the high-energy tail of the proton spectra at all angles. Experimental fragment spectra show a mid-rapidity component that is not reproduced by any of the models, although INCL++ is much closer to the data than the others. At large angles, the INCL++ spectra show a broad bump that is not seen in the data and that is the continuation of the projectile-like fragmentation peak at 4°. In other words, the projectile-like fragments seem to pick up too much transverse momentum from the collision, which results in a too broad angular distribution. This obviously indicates that the model fails to properly describe some aspects of projectile fragmentation.

D. Fragmentation cross sections

We finally turn to the analysis of fragmentation cross section. In keep with our approach to the validation of nucleon-induced reactions, we focus on measurements of isotopic cross sections in inverse kinematics. The advantage of such data sets is that they provide a comprehensive picture of the reaction mechanism. The accurate fragmentation data on hydrogen targets taken using the Fragment Separator at GSI (Darmstadt, Germany) [e.g. 25–27] have often proved invaluable for the study of the nucleon-nucleus reaction mechanism and for the optimization of de-excitation models.

Unfortunately, the coverage for reactions on light nuclei is not as extensive as for hydrogen. Beryllium has often been used as a production target in the search for exotic neutron-rich [e.g. 28–30] or neutron-poor [e.g. 31, 32]

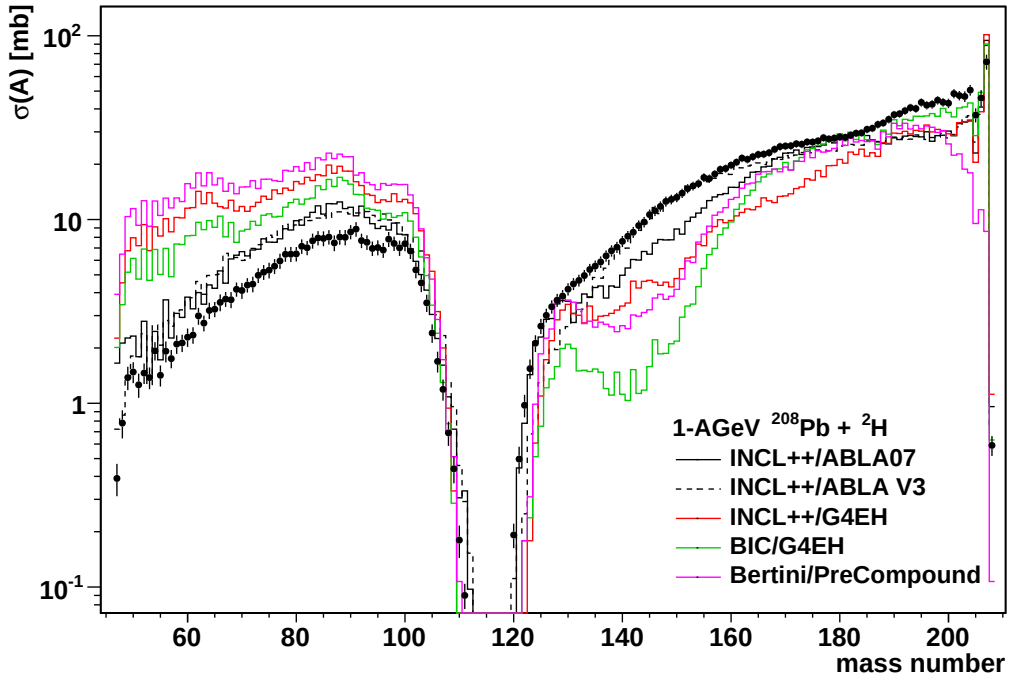

Figure 12: Fragmentation cross sections for the 1-*A*GeV ^{208}Pb+^{2}H reaction, as a function of the fragment mass number. Model calculations are compared to the data taken from Refs. 33 and 34.

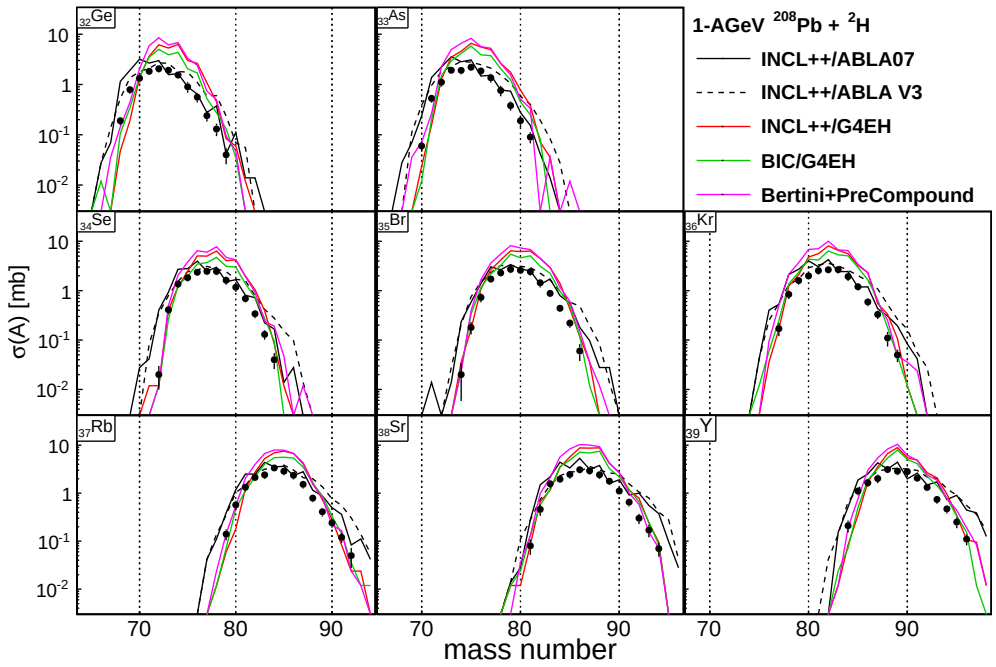

Figure 13: Isotopic distributions from the fission region ($32 \leq Z \leq 39$) for the 1-*A*GeV ^{208}Pb+^{2}H reaction. Model calculations are compared to the data taken from Ref. 33.

nuclei, but there exist only few experiments where essentially all projectile-like fragments were covered.

The data for 1 *A*GeV ^{208}Pb on deuterium [33], although only marginally relevant for the validation of INCL++'s nucleus-nucleus extension, are perhaps the most complete. Figure 12 shows the mass distributions of the fragments. Note that the model predictions are obtained by summing up the isotopic cross sections only over the isotopes that were detected in the experiment; this is the reason of the dip around $A = 115$.

One immediately observes that the model predictions are very sensitive to the choice of the de-excitation

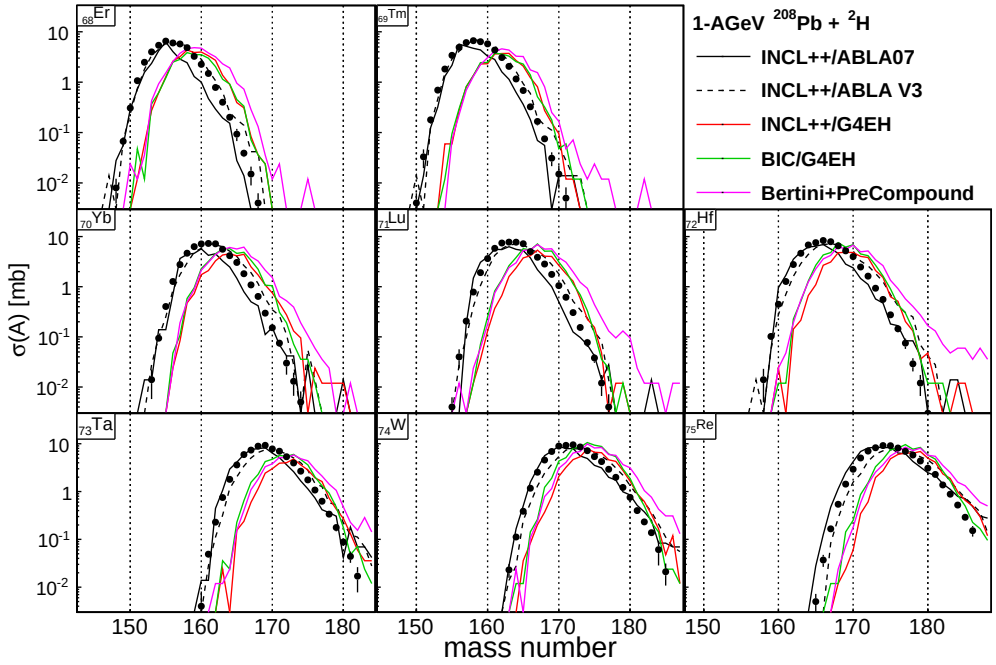

Figure 14: Isotopic distributions from the spallation region ($68 \leq Z \leq 75$) for the 1-*A*GeV ^{208}Pb+^{2}H reaction. Model calculations are compared to the data taken from Ref. 33.

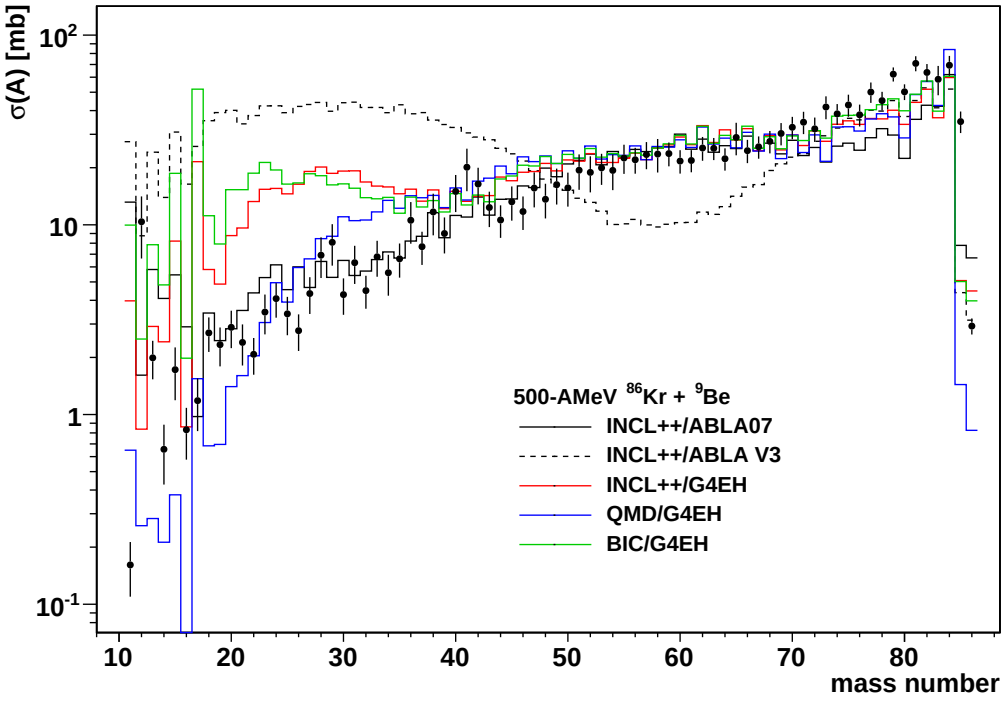

Figure 15: Fragmentation cross sections for the 500-*A*MeV ^{86}Kr+^{9}Be reaction, as a function of the fragment mass number. Model calculations are compared to the data taken from Refs. 37.

model. The distribution of spallation residues ($A > 115$) is accurately described only by INCL++/ABLA07 and INCL++/ABLA V3 (except very close to the projectile mass 208). Models coupled with G4ExcitationHandler systematically underestimate the yields for deep spallation residues ($115 < A \lesssim 160$). All the models overestimate the cross sections for the fission products ($A < 115$) by a factor of 2–4. This was already the case with INCL4.2 [35]. The overestimation of INCL++/ABLA07's and INCL++/ABLA V3's predictions should probably be related to the underestimation around $A = 195$; it has been shown [36] that fissioning nuclei belong exactly to this mass range.

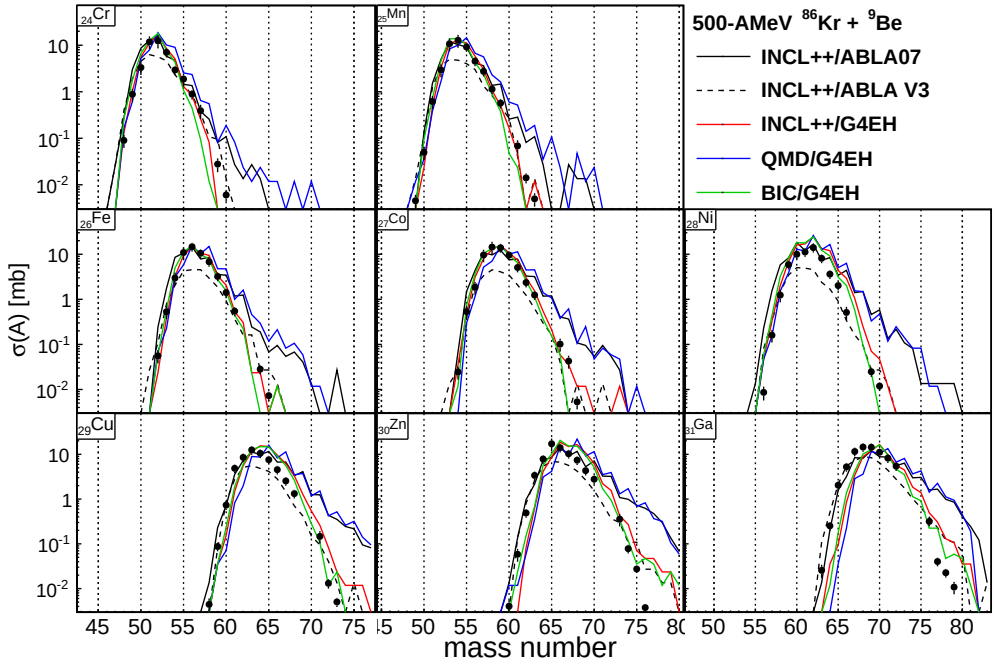

Figure 16: Isotopic distributions ($24 \leq Z \leq 31$) for the 500-*A*MeV ^{86}Kr+^{9}Be reaction. Model calculations are compared to the data taken from Ref. 37.

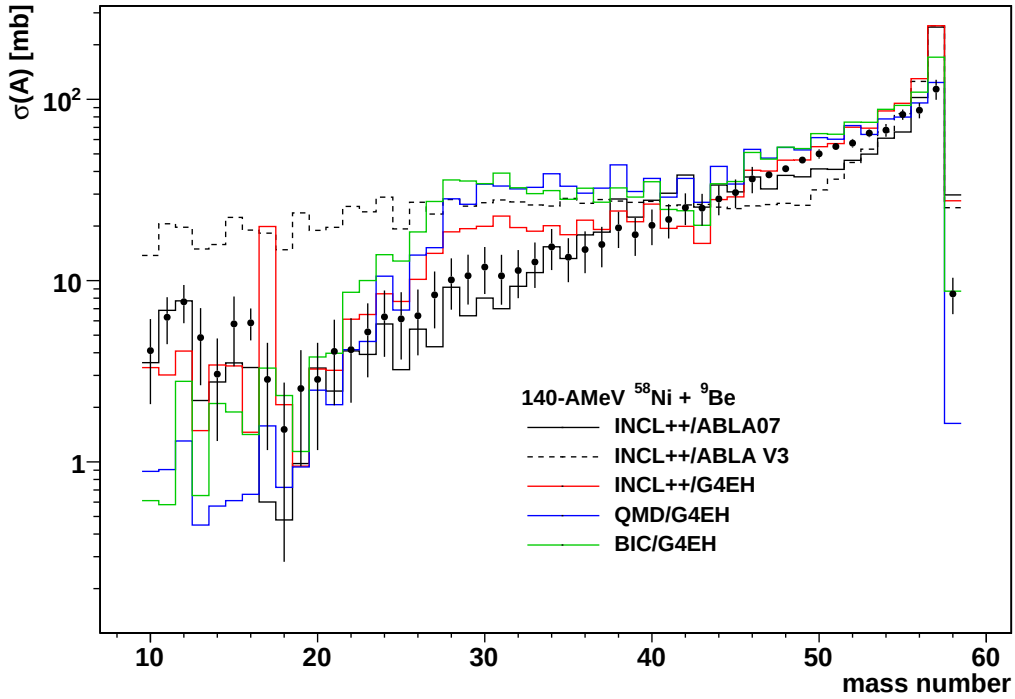

Figure 17: Fragmentation cross sections for the 140-*A*MeV ^{58}Ni+^{9}Be reaction, as a function of the fragment mass number. Model calculations are compared to the data taken from Refs. 38, 39.

Figure 13 shows a few isotopic distributions from the fission region. The INCL++/ABLA07 and INCL++/ABLA V3 predictions have more or less the correct shape but the wrong normalization, while the distributions predicted by G4ExcitationHandler and Bertini's fission module are systematically too narrow. This suggests that it should be possible to reproduce the data by acting on the competition between fission and evaporation in ABLA07 or ABLA V3.

Figure 14 shows some isotopic distributions in the region of the spallation residues. Again, the predictions by INCL++/ABLA07 and INCL++/ABLA V3 are rather close to the experimental data, while the other models systemati-

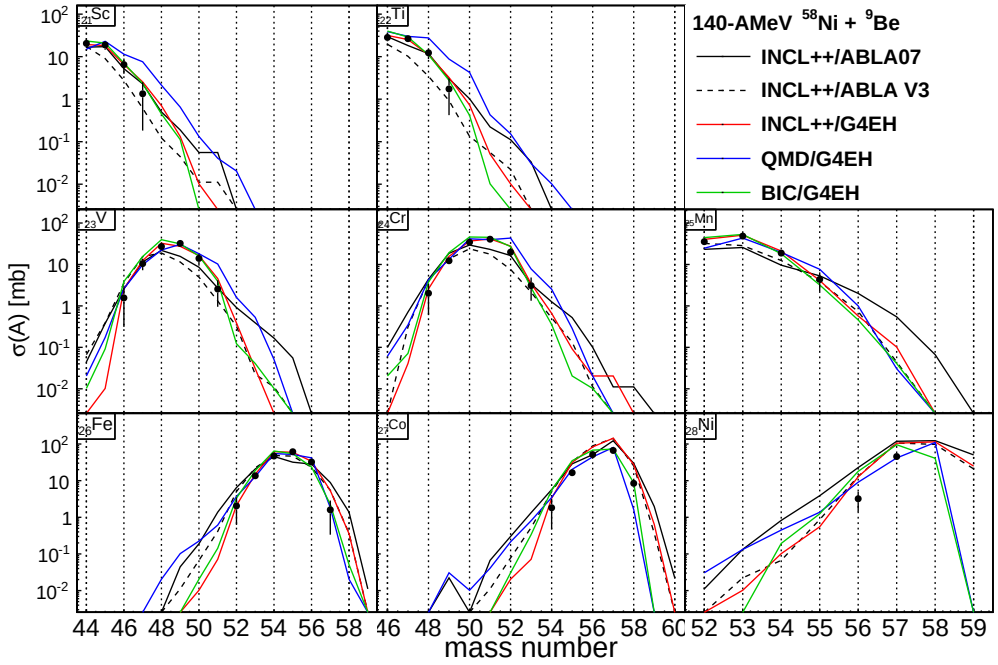

Figure 18: Isotopic distributions ($21 \leq Z \leq 28$) for the 140-*A*MeV ^{58}Ni+^{9}Be reaction. Model calculations are compared to the data taken from Refs. 38, 39.

cally overestimate the N/Z ratio of the residues.

As far as reactions on light nuclei are concerned, isotopic fragmentation cross sections have been measured by Weber *et al.* [37] for 500 *A*MeV ^{86}Kr+^{9}Be. We are aware of no other extensive measurement of isotopic fragmentation cross sections above $\sim$ 250 *A*MeV on a light target ($A < 18$). The mass distribution and some isotopic distributions are shown in Figs. 15 and 16. Again, note that the only *measured* isotopes contribute to the model predictions for the mass distribution.

The mass distribution of fragments is again mostly sensitive to the choice of the de-excitation model. The INCL++/ABLA07 can reproduce most of the experimental data fairly well, but it underestimates the production of fragments close to the projectile ^{86}Kr. QMD performs slightly better close to the projectile but slightly worse at intermediate mass ($A \simeq 35$). The INCL++/G4ExcitationHandler and BIC/G4ExcitationHandler couplings reproduce well the data for $A > 40$, but overestimate the cross sections for lighter fragments. The INCL++/ABLA V3 coupling, finally, largely overestimates the cross section for the lightest fragments.

The large difference between ABLA V3 and ABLA07 can be explained by the fact that evaporation channels in ABLA V3 are limited to proton, neutron and alpha. ABLA07, on the other hand, can simulate the emission of any fragment up to half of the mass of the excited nucleus. Also, G4ExcitationHandler can evaporate fragments up to ^{28}Mg and can be considered to be intermediate between ABLA V3 and ABLA07. Thus, the predicted cross sections in the $A < 40$ region seem to correlate well with the models' maximum ejectile mass. The QMD/G4ExcitationHandler coupling respects this trend to a degree for fragment masses above $\sim$ 25.

The isotopic distributions in Fig. 16 illustrate that INCL++/ABLA07 is affected by a defect. The yields for neutron-rich isotopes of $Z > 25$ nuclei are systematically overestimated. This defect might be correlated with the underestimation of the cross sections for the heaviest fragments. Given that ABLA07 is probably the most sophisticated of the de-excitation models considered, it would be tempting to conclude that defects in the predicted isotopic yields are actually due to intranuclear cascade. We already know that INCL++ neglects Pauli blocking on the first collision in the projectile and we have already mentioned (see Sec. III B above) that we expect this to be reflected by excess cross section in peripheral-reaction channels. The neutron-rich residues in Fig. 16 indeed correspond to peripheral reactions. However, the QMD/G4ExcitationHandler coupling is surprisingly affected by a very similar defect. It is also difficult to defend this conjecture if one observes that the other couplings to G4ExcitationHandler yield curves in reasonable agreement with the experimental data.

Similar conclusions can be drawn from the results at lower beam energy. We show in Figs. 17 and 18 the comparison between the model predictions and the experimental data for 140-*A*MeV ^{58}Ni+^{9}Be [38, 39]. Note that at this energy only about 10% of the reaction cross section is generated by INCL++'s low-energy fusion sector.

Again, most of the mass distribution is best predicted by INCL++/ABLA07, with the exception of nuclei close to the projectile ^{58}Ni. The INCL++/G4ExcitationHandler result is similar but slightly less good (the $A = 17$ cross section

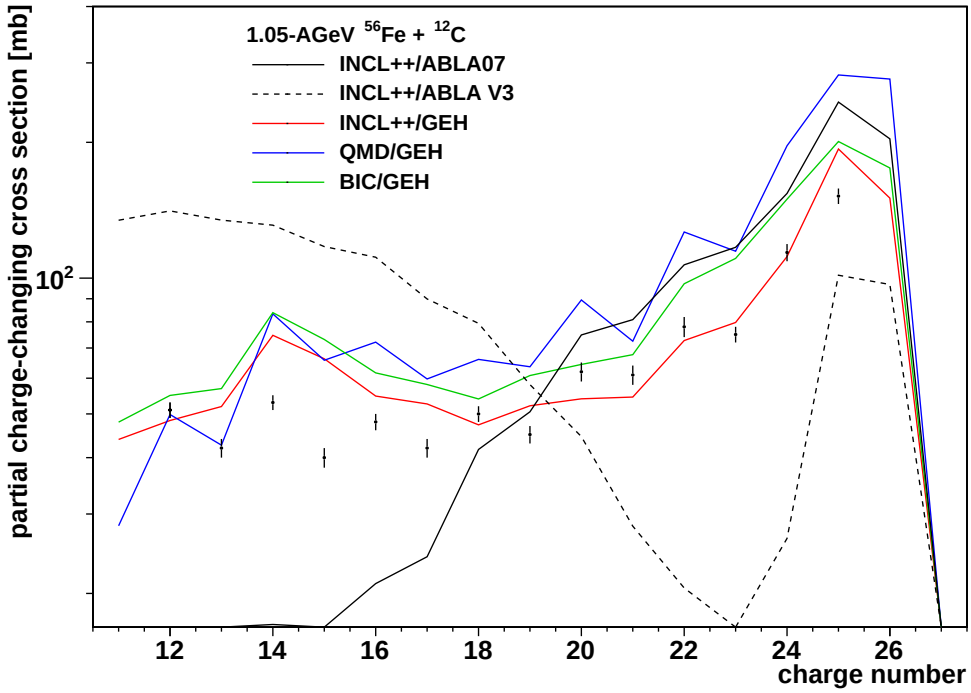

Figure 19: Partial charge-changing cross sections for the 1.05-*A*GeV ^{56}Fe+^{12}C reaction. Model calculations are compared to the data taken from Refs. 40.

is largely overestimated, but all the yield comes from the single isotope ^{17}O). The BIC/G4ExcitationHandler and QMD/G4ExcitationHandler couplings are yet less good, and INCL++/ABLA V3 is overall the worst. This is easy to understand if one remembers that ABLA V3 cannot evaporate intermediate-mass fragments, which occur most abundantly in light systems (such as ^{58}Ni and ^{86}Kr).

We have observed that the INCL++-based calculations systematically overestimate the cross sections for small mass losses. It is again tempting to interpret this in terms of lacking Pauli blocking on the first collision in the projectile Fermi sea. It will be interesting to verify this conjecture by refining the model.

The isotopic distributions in Fig. 18 are qualitatively similar to those of Fig. 16, but one has to bear in mind that the experimental coverage is less extensive here. It is difficult to verify if INCL++/ABLA07 and QMD/G4ExcitationHandler overestimate the yields for neutron-rich residues, as they do in 500-*A*MeV ^{86}Kr+^{9}Be.

We conclude our validation section by discussing the model predictions for partial charge-changing cross sections for a 1.05 *A*-GeV ^{56}Fe projectile colliding with a ^{12}C target [40]. Of all the reactions so far considered, ^{56}Fe+^{12}C is the one that leads to the highest excitation energies per nucleon, due to the high kinetic energy and the relatively small size of the projectile nucleus. At sufficiently large excitation energy, multifragmentation is expected to become the dominant de-excitation mechanism. Among the considered de-excitation models, ABLA07 is the only one to feature a semi-empirical treatment of multifragmentation. The G4ExcitationHandler model does include a multifragmentation module, but it is deactivated by default.

The model calculations are compared with the experimental data in Fig. 19. One remarks that the INCL++/ABLA V3 prediction is poor. We have already observed above that ABLA V3 is not suitable for systems for which there is a large probability of evaporating intermediate-mass fragments. The 1.05 *A*GeV ^{56}Fe+^{12}C reaction surely falls within this category. The INCL++/G4ExcitationHandler and BIC/G4ExcitationHandler predictions are quite similar and in good agreement with the data, while the QMD/G4ExcitationHandler cross sections are slightly too large. Finally, INCL++/ABLA07 is close to the experimental data for $Z \gtrsim 19$, but severely underpredicts the data for the smallest charges.

It is perhaps surprising to observe that the cross sections for large charge losses are best reproduced using de-excitation models that *neglect* multifragmentation. ABLA07 is the only model that somehow tries to handle this mechanism, but the comparison with the data seems to indicate that its semi-empirical treatment is inadequate for the large excitation energies that can be reached in this reaction. On the other hand, it is known that sequential binary decay can generate charge partitions that are similar to those generated by multifragmentation [41]. More discriminating observables would be needed to illustrate the difference between the two de-excitation modes.

IV. CONCLUSIONS

We have presented for the first time the new C++ incarnation of the Liège Intranuclear Cascade model, a solid, modern code which is intended to be used as the base for any future development. The INCL++ code is feature-wise and physics-wise equivalent to its Fortran counterpart as far as nucleon- and pion-induced reactions are concerned. In addition, INCL++ has been extended to simulate reactions induced by light ions (up to $A = 18$). We presented the validation of the extended model against experimental data for reaction, particle-production and fragmentation cross sections. We also compared the INCL++ results against other models in Geant4. The results are very encouraging. INCL++ is found to strike an excellent compromise between predictive power and CPU economy; compared to QMD the CPU time required by INCL++ is one to two orders of magnitude smaller. The comparison also highlighted a few shortcomings which will be dealt with in the future development.

[1] A. Boudard, J. Cugnon, J.-C. David, S. Leray, and D. Mancusi, Phys. Rev. C **87**, 014606 (2013), arXiv:1210.3498 [nucl-th].
[2] D. Mancusi, A. Boudard, J. Cugnon, J.-C. David, M. Hagiwara, and S. Leray, in *Proceedings to the Joint International Conference on Supercomputing in Nuclear Applications + Monte Carlo 2013* (Paris, France, 2013).
[3] S. Leray, J.-C. David, M. Khandaker, G. Mank, A. Mengoni, N. Otsuka, D. Filges, F. Gallmeier, A. Konobeyev, and R. Michel, J. Korean Phys. Soc. **59**, 791 (2011).
[4] J. Allison *et al.*, IEEE T. Nucl. Sci. **53**, 270 (2006).
[5] S. Agostinelli *et al.*, Nucl. Instr. Meth. A **506**, 250 (2003), official web site: `http://geant4.cern.ch/`.
[6] P. Kaitaniemi, A. Boudard, S. Leray, J. Cugnon, and D. Mancusi, Prog. Nucl. Sci. Technol. **2**, 788 (2011).
[7] M. Takechi, M. Fukuda, M. Mihara, *et al.*, Phys. Rev. C **79**, 061601 (2009).
[8] M. Fukuda, M. Takechi, D. Nishimura, *et al.*, in *Tours symposium on nuclear physics and astrophysics — VII*, AIP Conf. Proc., Vol. 1238 (AIP, Kobe, Japan, 2009) pp. 270–273.
[9] M. Takechi, *Elucidation of the behavior of reaction cross sections at intermediate energies and halo structure of* ^{6}*He*, Ph.D. thesis, Osaka University (2006).
[10] M. Takechi, M. Fukuda, M. Mihara, *et al.*, Eur. Phys. J. A **25**, 217 (2005).
[11] S. Kox, A. Gamp, C. Perrin, J. Arvieux, R. Bertholet, J. F. Bruandet, M. Buenerd, Y. El Masri, N. Longequeue, and F. Merchez, Phys. Lett. B **159**, 15 (1985).
[12] S. Kox, A. Gamp, R. Cherkaoui, A. J. Cole, N. Longequeue, J. Menet, C. Perrin, and J. B. Viano, Nucl. Phys. A **420**, 162 (1984).
[13] W. Shen, B. Wang, J. Feng, W. Zhan, Y. Zhu, and E. Feng, Nucl. Phys. A **491**, 130 (1989).
[14] Y. Iwata, T. Murakami, H. Sato, H. Iwase, T. Nakamura, T. Kurosawa, L. Heilbronn, R. M. Ronningen, K. Ieki, Y. Tozawa, and K. Niita, Phys. Rev. C **64**, 054609 (2001).
[15] L. Heilbronn, C. J. Zeitlin, Y. Iwata, T. Murakami, H. Iwase, T. Nakamura, T. Nunomiya, H. Sato, H. Yashima, R. M. Ronningen, and K. Ieki, Nucl. Sci. Eng. **157**, 142 (2007).
[16] J. M. Quesada, V. Ivanchenko, A. Ivanchenko, M. A. Cortés-Giraldo, G. Folger, A. Howard, and D. Wright, Prog. Nucl. Sci. Technol. **2**, 936 (2011).
[17] E. J. Moniz, I. Sick, R. R. Whitney, J. R. Ficenec, R. D. Kephart, and W. P. Trower, Phys. Rev. Lett. **26**, 445 (1971).
[18] G. Folger, V. Ivanchenko, and J. Wellisch, Eur. Phys. J. A **21**, 407 (2004).
[19] A. Heikkinen, N. Stepanov, and J. P. Wellisch, in *Proceedings to Computing in High Energy and Nuclear Physics 2003 (CHEP03)* (La Jolla, CA, U.S.A., 2003) p. MOMT008, arXiv:0306008 [nucl-th].
[20] M. Kelsey, D. Wright, *et al.*, in preparation (2014).
[21] K. K. Gudima, S. G. Mashnik, and V. D. Toneev, Nucl. Phys. A **401**, 329 (1983).
[22] J. Dudouet, D. Juliani, M. Labalme, *et al.*, Nucl. Instr. Meth. A **715**, 98 (2013), experimental data retrieved on 13$^{\text{th}}$ December 2013 from `http://hadrontherapy-data.in2p3.fr/`.
[23] J. Dudouet, D. Juliani, M. Labalme, *et al.*, Phys. Rev. C **88**, 024606 (2013).
[24] J. Dudouet, D. Cussol, D. Durand, and M. Labalme, Phys. Med. Biol. (2014), submitted, arXiv:1309.1544 [nucl-ex].
[25] P. Napolitani, K.-H. Schmidt, A. S. Botvina, F. Rejmund, L. Tassan-Got, and C. Villagrasa, Phys. Rev. C **70**, 054607 (2004).
[26] J. Benlliure, P. Armbruster, M. Bernas, A. Boudard, J. P. Dufour, T. Enqvist, R. Legrain, S. Leray, B. Mustapha, F. Rejmund, K.-H. Schmidt, C. Stéphan, L. Tassan-Got, and C. Volant, Nucl. Phys. A **683**, 513 (2001).
[27] T. Enqvist, W. Wlazło, P. Armbruster, *et al.*, Nucl. Phys. A **686**, 481 (2001).
[28] A. Stolz, T. Faestermann, J. Friese, *et al.*, Phys. Rev. C **65**, 064603 (2002).
[29] J. Benlliure, M. Fernández-Ordóñez, L. Audouin, *et al.*, Phys. Rev. C **78**, 054605 (2008).
[30] H. Alvarez-Pol, J. Benlliure, E. Casarejos, *et al.*, Phys. Rev. C **82**, 041602 (2010).
[31] B. Blank, S. Andriamonje, R. Del Moral, *et al.*, Phys. Rev. C **50**, 2398 (1994).
[32] J. Kurcewicz, Z. Liu, M. Pfützner, *et al.*, Nucl. Phys. A **767**, 1 (2006).
[33] T. Enqvist, P. Armbruster, J. Benlliure, *et al.*, Nucl. Phys. A **703**, 435 (2002).
[34] A. Kelić, K.-H. Schmidt, T. Enqvist, *et al.*, Phys. Rev. C **70**, 064608 (2004).
[35] A. Boudard, J. Cugnon, S. Leray, and C. Volant, Phys. Rev. C **66**, 044615 (2002).
[36] J. Cugnon, T. Aoust, and A. Boudard, in *Seminar on Fission VI*, edited by C. Wagemans, J. Wagemans, and P. D'Hondt (2008).
[37] M. Weber, C. Donzaud, J. Dufour, *et al.*, Nucl. Phys. A **578**, 659 (1994).

[38] M. Mocko, M. B. Tsang, L. Andronenko, *et al.*, Phys. Rev. C **74**, 054612 (2006).
[39] M. Mocko, *Rare isotope production*, Ph.D. thesis, Michigan State University, East Lansing, MI, U.S.A. (2006).
[40] C. Zeitlin, L. Heilbronn, J. Miller, S. E. Rademacher, T. Borak, T. R. Carter, K. A. Frankel, W. Schimmerling, and C. E. Stronach, Phys. Rev. C **56**, 388 (1997).
[41] D. Mancusi, A. Boudard, J. Cugnon, J.-C. David, T. Gorbinet, and S. Leray, Phys. Rev. C **84**, 064615 (2011), arXiv:1110.6343 [nucl-th].